iJRASET
International Journal For Research in Applied Science and Engineering Technology

INTERNATIONAL JOURNAL FOR RESEARCH

IN APPLIED SCIENCE & ENGINEERING TECHNOLOGY

Volume: 13 **Issue:** VII **Month of publication:** July 2025

DOI: https://doi.org/10.22214/ijraset.2025.73196

www.ijraset.com

Call: 08813907089 | E-mail ID: ijraset@gmail.com

International Journal for Research in Applied Science & Engineering Technology (IJRASET)
ISSN: 2321-9653; IC Value: 45.98; SJ Impact Factor: 7.538
Volume 13 Issue VII July 2025- Available at www.ijraset.com

Observational Insights of Solar-Terrestrial Coupling from the Ionospheric and Surface Impacts during Solar Perturbations

Abhijit Banerjee[1], Rina Bhattacharya[2]
Department of Physics, JIS University, 81, Nilgunj Road, Agarpara, West Bengal, Kolkata 700109, India

Abstract: ***We investigated three intense solar–terrestrial disturbance chains in 2022 viz. an X1.5 flare on February 15, an X1.0 + M8.7 flare based CME sequence on October 2 and a G3-geomagnetic storm driven by multiple CMEs on October 4 thereby aiming to diagnose how impulsive solar energy input cascades through the coupled ionosphere and troposphere system. Multi-platform data sets were used: GOES/SDO EUV–X-ray fluxes, ESA Solar Orbiter imagery, SWPC solar-wind and IMF parameters, ground-based ionosondes (TEC, N_mF_2, Ne, f_0F_2) and surface meteorological records. Results reveal a spectrum of responses governed by event type and magnetic field geometry. Immediate ionospheric impacts show a TEC bulge within < 5 min and peak N_mF_2/f_0F_2 at 16:00 UT. These were exclusive to the Earth-pointing X1.0 flare on October 2, neither the backside X1.5 flare nor the geomagnetic storm responsible for the production of such daytime surges. Ring current and TEC coupling was strongest on October 2. B_z minima (-8 nT) coincided with a 588 km s^{-1} solar-wind stream, yielding the highest polynomial 0^{th} and 1^{st} coefficients in TEC-Dst hysteresis loops. Storm scale forcing on October 4 manifested as sustained K_p = 7 and deep polar-cap absorption though the correlation of flare flux with K_p as low. Joule heating driven gravity-wave packets elevated high latitude surface pressure by 2–3 hPa and enlarged standard deviations of TEC and N_mF_2. Back-side eruptions on February 15 generated a negligible tropospheric or ionospheric change despite of a 3 Mkm prominence; SUVI-STEREO imagery confirmed the eruption's off-disk trajectory thereby highlighting geo-effective line-of-sight requirements. Surface meteorology echoed upper-atmosphere forcing as the X1.05 flare embedded in the October 2 sequence cooled near-surface air and dew point while raising humidity and pressure, consistent with rapid modulation of the global atmospheric-electric circuit. Collectively, the study demonstrates that only Earth directed, magnetically connected sources drive coherent, multi-layer perturbations. Event specific lag signatures as in minutes for flare ionization, in hours for CME ion-drag heating and days for storm time gravity-wave coupling so these are critical to forecasting technology relevant ionospheric gradients and extreme weather precursors.***

Keywords: Solar flare, CMEs, Solar-Terrestrial coupling, TEC and Geomagnetic storm

I. INTRODUCTION

A solar flare is a phenomenon on the solar surface characterized by the impulsive release of energy. Solar flares are associated with the coronal mass ejections. Where the solar magnetic and its embedded particles are thrown into the interplanetary space and solar environment. The modifications in the solar wind density with magnetic field alignment strength are occurred during the activity [1]. In the ionosphere over the Earth's surface dynamo process is executed due to the flow of plasma current and thereby its magnetic field. At the solar perturbation, intervention of variable solar magnetic field and modifications in the solar proton density, the dynamo process is disturbed [2,3]. Solar flares are originated from the active places of sunspots [4]. At the vicinity of several sunspots the flares are generated. Some of these flares use to face the Earth [5]. At this perturbation in the Earth atmosphere is located and the intensity of the solar flare is measured through the Geo-synchronous observatory environmental satellites (GOES) in the X-ray band [6]. For the last few decades, Sun is flaring more and more towards the approaching of the solar maxima in the eleven-year solar cycle and during the year 2022, these flaring events get more pronounced. There is continuous burst from the solar corona due to the magnetic activity. These burst instigates the solar plasma with magnetic fields into the interplanetary space [7]. These are resulted into the CMEs, following which the collision of the solar ejecta and Earth's magnetic field is happened there by causing a geomagnetic storm [8].

In this context on February 15, 2022 at 1815 UT, the European Space Agency reported that its solar orbiter spacecraft captured the longest solar prominence together with the full solar disk [9]. That prominence was about 3 million km long, which covers approximately 250 times diameter of Earth. The prominence has originated on the Earth's opposite side sun. An X class-flare, the most powerful category of solar flare has supposed to appear in this event. Prominences like this one are huge structures on our local star, made of superheated gas called plasma, intertwined with solar magnetic fields. These are commonly called CME's, existing as enormous filling of the plasma and sometimes directed towards Earth [10]. The sunspot AR2941 is generated this M-class solar flares. The category was M1.3 explosions with a minor shortwave radio blackout over South America is reported [11].

On October 2, 2022 a giant class of strong solar flare is observed through solar dynamics observatory (SDO) where X1.0 class of flare is observed peaking at 4.25 p.m. in EDT [12,13]. It is detected from the AR3110 less active region of the Sun where from this X1-class solar flare is generated. Pacific Ocean and few parts of North America had experienced shortwave radio blackout is generated as reported from the flare images. As per the usual processes, there should be a throughput of the CMEs into the space.

On October 4, 2022 a prediction of generation of G2- class of geomagnetic storm along with the overlapping of multiple CMEs with the Earth's magnetic field is reported by National Oceanic Atmospheric Association (NOAA) [14,15]. A strong group flares is reported to be generated from the sunspot AR3110 due to constant obstruction of CMEs done by this sunspot. The newly form AR3112 sunspot is also considered during these prediction as this spot is fully grown and through the month of October its shows high level of activity and faced the Earth at its transits on the solar disc. Solar flare affects the various ionospheric parameters in considerable amount of which F_2 agitated most, as it positioned extreme externally among all the layers.

The surface layer parameters are also affected from the particles and the field emitted from the solar radiation during flare. Coronal mass ejections (CMEs), solar-flare effects (SFEs) and the geomagnetic storms can disturb not only the ionosphere but also the lowest layers of the atmosphere. When an Earth-directed CME compresses the magnetosphere the Joule heating and particle precipitation, inject energy that cascades downward as gravity-wave packets [16]. A statistical study in Antarctica documented measurable rises in near-surface temperature, humidity and cloud cover within 2–3 days of sustained ultra-low-frequency geomagnetic activity associated with storms [17]. During strong flares, sudden bursts of X-ray and EUV flux modify the global atmospheric-electric circuit. The balloon and ground sensors record these brief fluctuations in surface potential gradient and pressure attributable to the extra ionization [18]. The crochet-like magnetic signature that defines an SFE provides a precise timing marker for these electrodynamic changes and links them to flare onset [19-22].

In this work, we have analysed these three categories of solar perturbations from the aspects of meteorological and ionospheric radio data on surface and ionosphere F_2 layer respectively. Some of the observational significant insights as obtained from this part of the analyses during those perturbations are as follows

1) February 15, 2022: X1.5 and M-class flares, Associated CME arrival time: 17.5 hours post-flare resulted in K_p=6 geomagnetic storm,.
2) October 2, 2022: M8.7 Flare, CME release for which a notable ionospheric onset <5 min is observed and tropospheric pressure anomalies
3) October 4, 2022 Geomagnetic Storm (G3-Class), Triggered by CME from September 30 AR13141 flare complex, Sustained K_p=7 conditions for 9 hours, deep polar cap absorption (PCA) event, Mid-latitude TEC enhancements >20 TECu and Surface pressure anomalies of 2-3 hPa at high latitudes.

Therefore, the present study carried out to analyse the observational insights that yields interesting results as a sign of solar-terrestrial coupling from the impacts on the parameters ionopsheric and surface layers on the solar perturbation events.

II. DATA ANALYSIS

A. *Observation from Space Probes*

Following tabular representation shows the detail of the space probe borne observatories and their on board instruments through which the radio data are received for the solar perturbation events on February 15 and October 2 and 4, 2022

TABLE I

DETAILS OF THE INSTRUMENTS AND OBSERVATORIES BORNE BY SPACE PROBES FOR THE RECEIVED RADIO DATA

Feature	LASCO C2 [23]	LASCO C3 [23]	AIA 304[24]	AIA 131[24]	AIA 171[24]	EUI/FSI (Solar Orbiter)
Platform	SOHO	SOHO	SDO	SDO	SDO	Solar Orbiter

Observation Type	White-light coronagraph	White-light coronagraph	EUV imaging	EUV imaging	EUV imaging	EUV wide-field imaging
Wavelength	~400–700 nm	~400–700 nm	304 Å (He II)	131 Å :Fe VIII-XXI	171 Å : Fe IX	174 Å :Fe IX
Temperature Sensitivity	Not temperature-specific	Not temperature-specific	~50,000–80,000 K	~0.4 MK and ~10 MK	~0.6 MK	~0.8 MK
Field of View	1.5–6 $R_{\odot}$	3.7–32 $R_{\odot}$	Full solar disk (~1.3 $R_{\odot}$)	Full solar disk (~1.3 $R_{\odot}$)	Full solar disk (~1.3 $R_{\odot}$)	Full solar disk + corona (~3.5 $R_{\odot}$)
Layer Observed	Inner corona	Outer corona / heliosphere	Chromosphere & transition region	Hot flare regions	Quiet corona and transition	Corona (large-scale EUV structures)
Primary Applications	CME onset, streamers	CME propagation, comets	Prominences, filaments, flare ribbons	Flare loops, hot plasma	Coronal loops, coronal holes	Wide-field view of coronal eruptions
Pulse/Cadence	~12–20 min	~30 min	12 sec	12 sec	12 sec	~5 min typical (varies with mode)
Resolution	~56 arcsecpixel^{-1}	~118 arcsecpixel^{-1}	0.6 arcsecpixel^{-1}	0.6 arcsecpixel^{-1}	0.6 arcsecpixel^{-1}	~5.6 arcsecpixel^{-1} (for full-disk FSI)

"SOHO: Solar and Heliospheric Observatory", "SDO: Solar Dynamics Observatory LASCO C2 and C3: Large Angle Spectroscopic Coronagraph Camera 2 and 3", "AIA: Atmospheric Imaging Assembly; EUI: Extreme Ultraviolet Imager", "FSI: Full Sun Imager", $R_{\odot}$: Solar radius, 1MK:100000K, 1 arcsecpixel^{-1} = 1/3600 of a degree

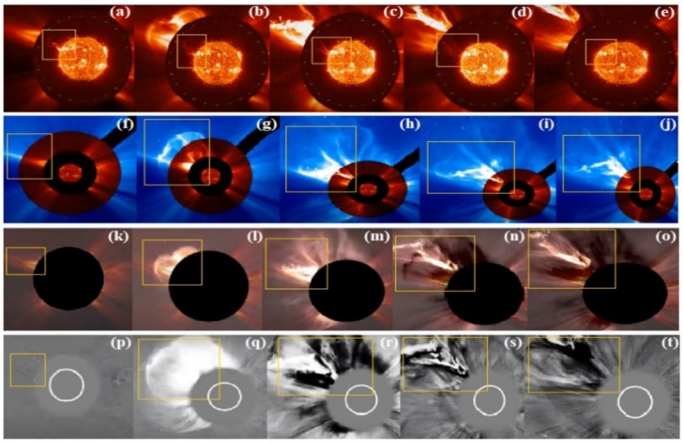

Fig. 1 Image of solar flare prominence on Feb 15, 2022 (a) to (e) from the FSI (EUI) (images of the solar disc spread about 3.5 million kilometers into the space shown by the center image), (f) to (j) from the LASCO-C2, LASCO-C3 and AIA 304, (k) to (o) from LASCO-C2 and LASCO-C3 and p to t from LASCO-C2. (SOHO and LASCO C2 imagery is superposed) [Courtesy: SOHO/ LASCO consortium. SOHO (ESA and NASA), www.helioviewer.org]

The Figure 1 shows Solar Orbiter spacecraft, imaging part captures the solar disc and about 3.5 million kilometers spreading in space located by the center image. With this C2 imagery of LASCO instrument of SOHO is superposed for further tracing.

It is reported by the several space organisations that on October 4, 2022 that few faster moving CMEs are emitted from the Sun's surface and those will be overtaken by the following giant CME's. The emitted space cloud from that CME contains the combinations of cloud and twisted magnetic fields that can generate the sparking auroras. This kind of CME is marked as Cannibal CME. The geomagnetic storm level approaches up to category G2 at this strike. This generates the Pink auroras as they occur in rare [25]. Another class of auroras are in nature of pulsations they are also rare. Mysterious pulsating auroras are also linked as Earth magnetosphere "chorus waves" [26,27]. On the night of Oct 4, 2022 in Abisko in Sweden, the sky watchers observed both the classes of CMEs at that duration. The time variant images of which is generated as shown by Figure 3 from the photography of Miquel Such [28]. The occurrence of the Pink auroras happens when solar wind particles penetrate deep enough into the Earth's atmosphere, while striking the molecular nitrogen less than 100 km above Earth's surface [25].

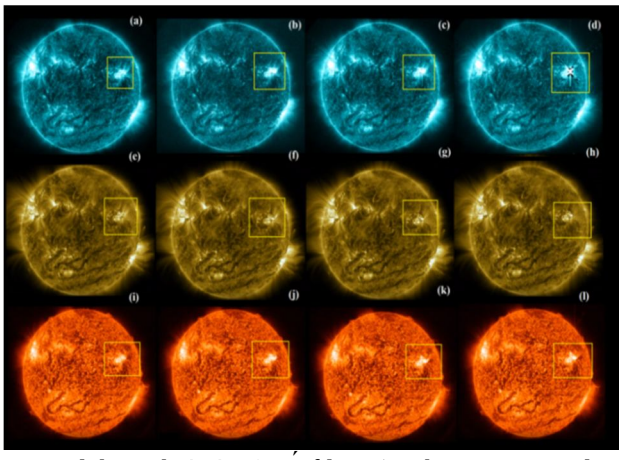

Fig. 2 Image of solar disc with flare a to d through AIA-131 ´ filter, (Dark area surrounding the flare event is shown after the correction process by utilising point spread function), e to h through AIA-171 ´ filter and i to l through AIA-304 ´ filter on October 2, 2022, 20.27.30 TAI (International Atomic Time) [13]

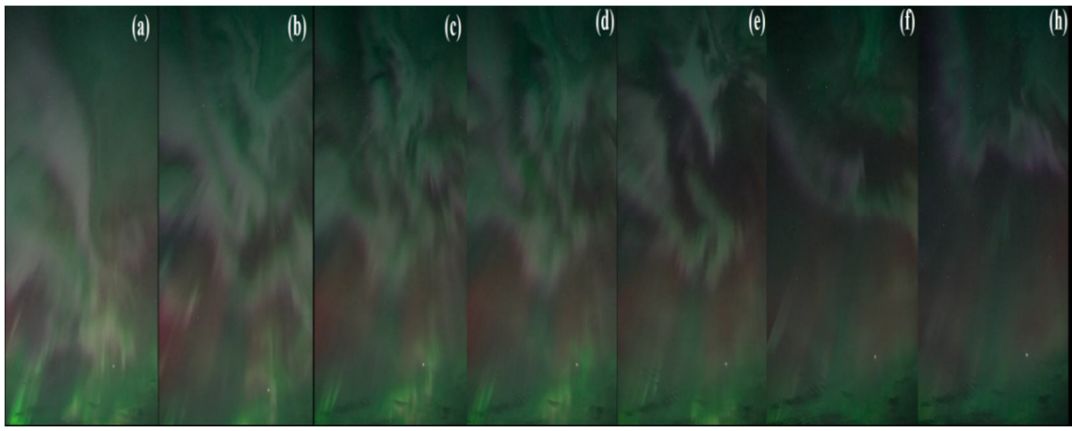

Fig.3 Pink auroras and pulsating auroras, Abisko, Sweden, sky watchers witnessed both rarities at the same time on October 4, 2022. (Picture credit: Photographed the display and created this time lapse, Miquel Such [28]

It is clear from the above observation that a breakage in the Earth's magnetic field on October 3, 2022 (as the observations in present analyse are taken for October 2 and 4, 2022) was appeared and the particles are able to reach that said near Earth level.

B. Observational and data driven analysis of solar events

The location based on which this study is done is Kolkata (West Bengal in India) with Latitude: 22.6^0, longitude: 88.4^0 and altitude: 300 km. The days are considered here for the analysis are October 2, 2022, October 4, 2022 and February 15, 2022. The parameters of the ionopsheric-layer are obtained from the Ionosondes and Scattering Radars data. These data are the collected from the International Reference Ionosphere (IRI): CCMC,GSFC (NASA) Model:2020.

These data are taken for the 0.1 sec resolution in the time scale and the ranges of data sets are 50 to 15,000 kms. The TEC, f_0F_2, Ne and N_mF_2 are considered here. In the geomagnetic activity, the parameters like three hours K_p index and derived A_p and C_p indices are considered here. These geomagnetic data are collected from GFZ Helmholtz Potsdam, Germany. The K_p, A_p, C_p indices and 24 hrs. Dst index are considered here for the said days. Dst index is collected from University of Kyoto. The X-band solar data is collected from Geosynchronous Orbiter Environmental Satellites (GOES) of National Oceanic Atmospheric Authority (NOAA). The L-band communications of these satellites are done from the space to Earth. These GOES scale classification ranges as $10^{-7}<B<10^{-6}$, $10^{-6}<C<10^{-5}$, $10^{-5}<M<10^{-4}$ and $10^{-6}<X<10^{-5}$. The surface meteorological data are collected from Wyoming University.

TABLE III
DETAILS OF THE FLARE HAPPENED ON THE PERTURBED DAYS

Dates	Flares		Most intensified class of flares				Back ground flux
	Class	Numbers	Magnitudes	Starting	Peak	End	
October 2, 2022	C	10	C8.9	14:48	14:57	15:12	C1.47
			C9.2	22.49	23.08	23.19	
	M	3	M1	15:34	15:45	15:53	
			M1.2	13:52	14:05	14:23	
			M8.7	02.08	02.21	02.26	
	X	1	X1.05	19.53	20.25	20.34	
October 4, 2022	C	5	C4.4	00:37	00.43	00.56	C1.14
	M	1	M1.61	12.48	13.15	13.51	
February 15, 2022	C	3	C4.8	05:12	05.18	05.22	B4.18
	M	1	M1.3	17:54	18.15	18.31	

The differential variation of solar flare and TEC's are estimated *w.r.t.* their starting (s) to maximum (m) and maximum to ending (e) times using the following expressions

$$\Delta I'_{p,m-s} = \frac{\Delta I_P}{\Delta t}\Big|_{s-m} = \frac{I_{p,m}-I_{p,s}}{t_m-t_s}$$
$$\Delta I'_{p,m-e} = \frac{\Delta I_P}{\Delta t}\Big|_{m-e} = \frac{I_{p,m}-I_{p,e}}{t_m-t_s}$$
$$\Delta F'_{m,m-s} = \frac{\Delta F_m}{\Delta t}\Big|_{s-m} = \frac{F_{m,m}-F_{m,s}}{t_m-t_s}$$
$$\Delta F'_{m,m-e} = \frac{\Delta F_m}{\Delta t}\Big|_{m-e} = \frac{F_{m,m}-F_{m,e}}{t_m-t_s}$$

The ionospheic parameters are symbolises by I_P. The ionospheric parameters (p) used in this analysis are TEC, N_mF_2 and f_0F_2 and their denotations for maximum, starting and ending flare time are $I_{p,m}$, $I_{p,s}$ and $I_{p,e}$ respectively. Flare magnitude at the maximum, starting time and ending time denoted by $F_{m,m}$, $F_{m,s}$ and $F_{m,e}$ respectively. The transiency characterisation (I_{Tr}) of the ionospheric parameters and flare magnitude is estimated as follows.

$$I_{Tr} = \frac{\Delta I_p{}'}{\Delta F_m{}'}$$

Differential change in the parameter values and flare magnitude are represented by ΔI_P and ΔF_m.
The correlation characteristics for geomagnetic parameters K_p and the solar flares and Dst with TECs are evaluated here. The best fitted polynomial obtained by analysing the trend equations estimated from the correlated data points of the ionsopheric and geomagnetic variables is expressed as

$$y = a_0x^4 + a_1x^3 + a_2x^2 + a_3x^1 + a_4x^0$$

a_0, a_1, a_2, a_3 and a_4 are the coefficients and x is the independent variable.

III.RESULT AND DISCUSSION

Results obtained from the observational and data driven analysis of solar events and are given below

A. Solar Flares And Interplanetary Magnetic Fields

Following results show the details of solar flares happened on October 2, 2022, October 4, 2022 and February 15, 2022.

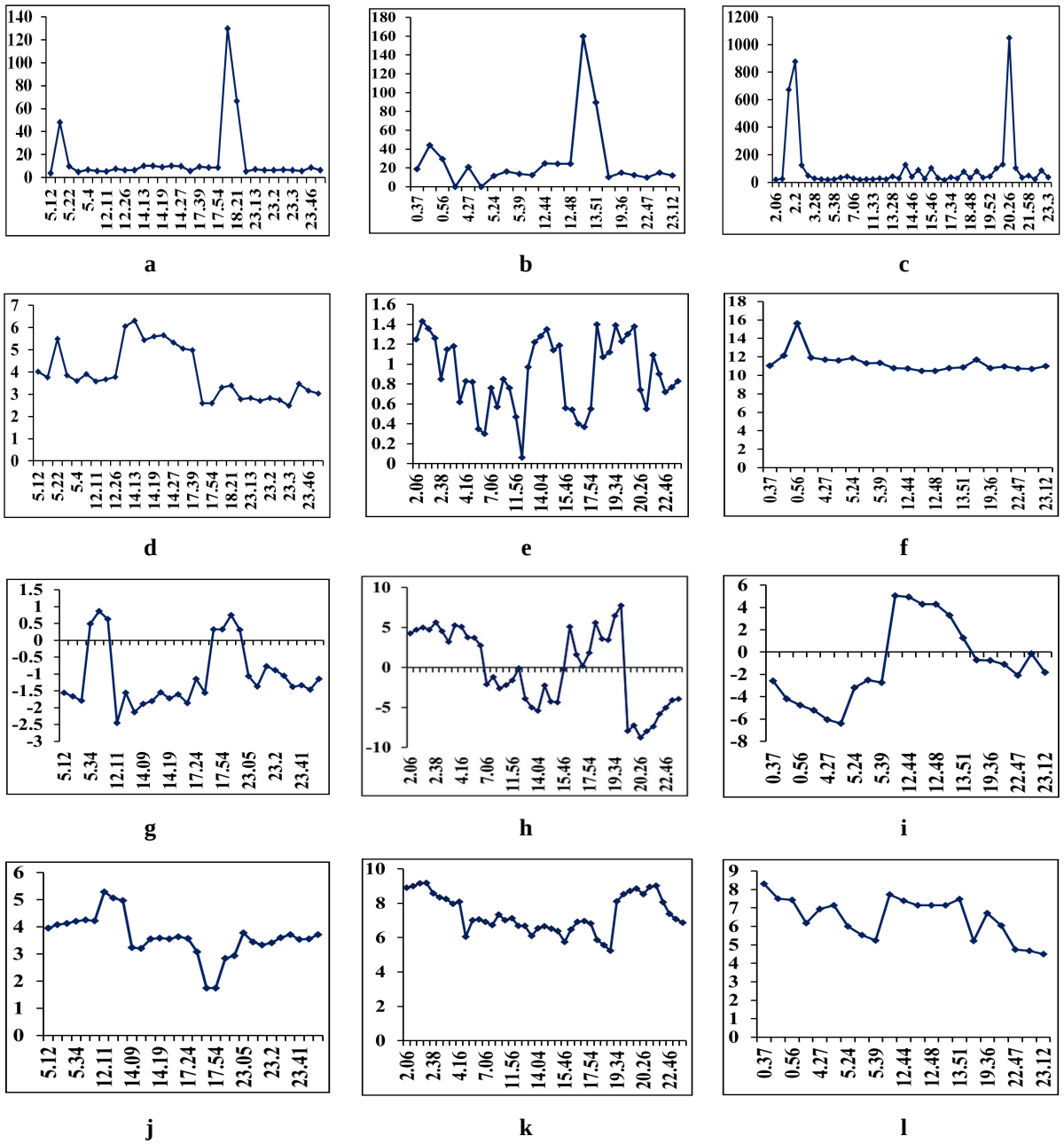

Fig.4 Diurnal variations of Flare magnitudes along ordinate (Wm^{-2}) (a) Feb 15, 2022, (b) Oct 2, 2022, (c) Oct 4, 2022; Solar wind particle density ($particlescm^{-3}$) (d) Feb 15, 2022, (e) Oct 2, 2022, (f) Oct 4, 2022; Z-component of interplanetary magnetic field (IMF in nT) (g) Feb 15, 2022, (h) Oct 2, 2022, (i) Oct 4, 2022, total component of interplanetary magnetic field (IMF in nT) (j) Feb 15, 2022, (k) Oct 2, 2022, (l) Oct 4, 2022 vs. Universal Time along abscissae.

TABLE IIIII

DESCRIPTIVE ANALYSIS OF THE SOLAR AND IMF COMPONENTS DURING SIGNIFICANT FLARES

Days of Flare	Significant Solar Flare classes and values	Solar wind density in pfu			Magnetic field Z component (B_Z) in nT			Magnetic field T component (B_T) in nT		
		I	II	III	I	II	III	I	II	III
Oct 2, 2022	C8.9	1.2	0.76	1.06	-2.17	-4.5	-5.35	6.6	6.58	6.1
	C9.2	0.66	0.59	0.7	-5.07	-4.17	-4.3	7.41	7.2	7.01
	M1.2	1.22	1.28	1.71	-4.33	-5.4	-4.53	6.42	6.58	6.4
	M1	1.13	0.53	1.12	-3	0.64	4.65	6.22	5.82	4.89
	M8.7	1.11	1.39	1.18	2.76	5	4.56	8.66	9.14	8.87
	X1.05	1.23	0.85	1.05	-7.97	-8.52	-8.26	8.69	8.82	8.37
Oct 4, 2022	C4.4	11.06	12.15	15.62	-2.56	-4.18	-4.76	8.3	7.51	7.43
	M1.61	10.46	10.79	10.89	4.3	3.29	1.27	7.15	7.15	7.49
Feb 15, 2022	C4.8	4.01	3.76	5.49	3.96	4.08	4.13	-1.56	-1.66	-1.79
	M1.3	2.6	3.3	3.63	0.32	0.75	0.81	1.75	2.84	3.75

Solar flares I: Starting time; II: Peak time; III: End time

TABLE IV

DESCRIPTIVE STATISTICS SOLAR WIND DENSITY AND IMFS

Parameters	Days	Solar wind density in pfu	Magnetic field Z component (B_Z)in nT	Magnetic field T component (B_T) in nT
Standard deviation	Feb 15, 2022	1.17	0.77	0.95
	Oct 2, 2022	1.10	1.13	3.63
	Oct 4, 2022	0.36	1.10	4.79
Mean	Feb 15, 2022	3.93	3.63	-1.03
	Oct 2, 2022	11.36	6.49	-0.99
	Oct 4, 2022	0.91	7.40	-0.12

B. Geomagnetic Parameters

The following contour plot shows the percentage distribution of prediction of the geomagnetic storms from October 2 to 4, 2022 and February 14 to 16 as per the Geophysical report published by NOAA, USA.

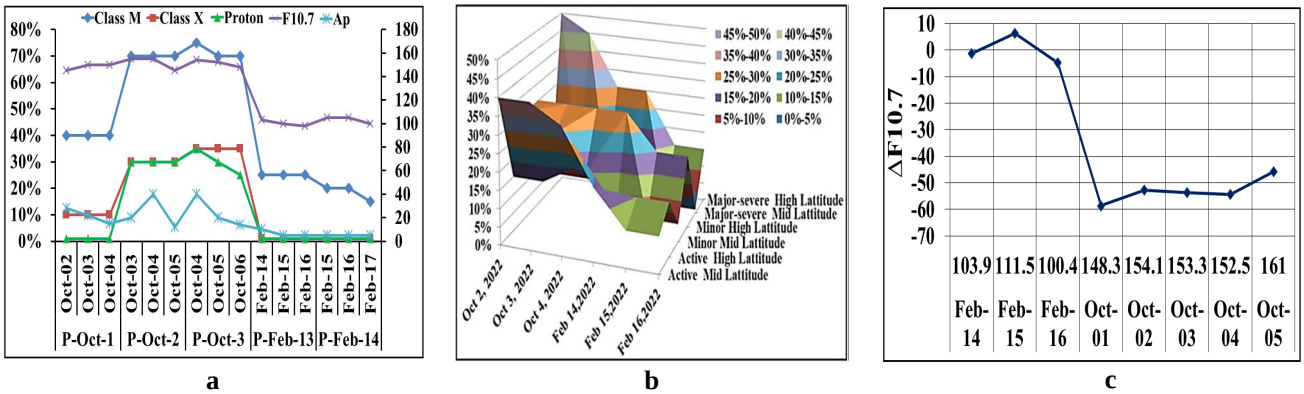

a **b** **c**

Fig. 5 (a) Event probabilities (P) of the class M, X and protons (left ordinate), prediction of F10.7 and A_p index (right ordinate), centring the flare days Oct 2, 4 and Feb-15, 2022, (b) Contour plot of prediction on geomagnetic storm from Oct 2 to 4 and Feb 14 to 16, 2022 (Data source: NOAA) and (c) Variation of F10.7 flux for the period Feb 14 to 16 and Oct-1-5, 2022 (Data source: NASA).

The event probabilities (P) of the class M, X and protons and the predicted values of F10.7 and A_p index for the time period involving the flares days are shown in Figure 5 (a). The distributions of active storms and major to severe storm are shown as more than 45% on Oct 2, 2022. A few coronal mass ejections and G2 class storm are predicted on Oct 4, 2022. On Oct 4, 2022, 35%-40% major severe mid latitude and major severe high mid latitude and 30%-35% shares are shown. On Feb 15, 2022, 15-20% of shares are shown in the figure for the major severe mid latitude. For the based suited purpose of interpretation the range of days including the days of interest are considered. The F10.7 radio burst shows enhancement in the level in +10 values for Feb 15, 2022. The radio flux is enhancing as the October month approaches. The variation of -50 to -60 from the average value of the flux value is observed.
In the following part of the analysis, the geomagnetic parameters are analysed to represent the prediction results.
Following are the variations obtained from the 3 hrs. K_p index. Derived A_p and C_p indices *w.r.t* period of days from February 14 to 16 and October 1 to 5, 2022 and also thee Dst index.

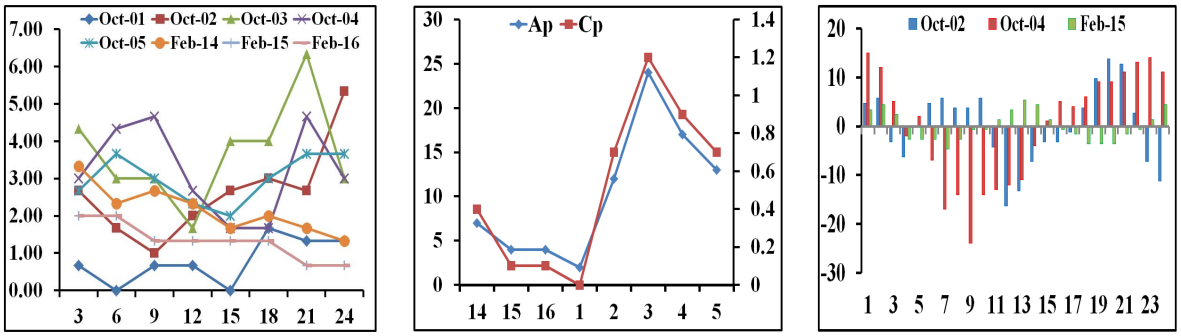

a **b** **c**

Fig.6 Variation of (a) K_p index vs. 3 hrs. Period, (b) A_p (ordinate right side), C_p (ordinate left side) values for the days Feb 14 to 16 and October 1 to 5 (absiaasae in days values) and (c) variation of Dst index vs. time in hour

The highest variation of K_p index is observed in Oct 2, 2022 is 5.33 at the X1 class of flare for the period 18 to 21 UTC. During Oct 4, 2022 maximum value is observed as 4.67 and on February 15 its stand as 2. During the considered period of Oct 1 to Oct 5, 2022 and February 14 to 16, 2022 the highest K_p index recorded on Oct 3, 2022 as 6.33. For the three flare days Oct 4, 2022 shows greater change in A_p and C_p indices as 17 and 0.9. Again, Oct 3, 2022 stood highest in the A_p and C_p index values among others. The average variation of 24 hrs Dst index for the three days shows that the most disturbed day can be considered as the Oct 4, 2022. The ascending order of maximum change in Dst index occurred as |-39|, |-30| and |-10| in Oct 4, Oct 2 and Feb 15, 2022 respectively. The following table 5 shows the statistical measures of the mean and standard deviations.

TABLE V
STATISTICAL MEASURES OF GEOMANTIC INDICES

Measures	October 2, 2022		October 4, 2022		February 15, 2022	
	Dst	K_p	Dst	K_p	Dst	K_p
Mean	-8.75	2.63	-21.04	3.21	-4.38	1.33
Standard Deviation	7.81	1.28	11.43	1.23	3.06	0.50

The correlation of K_p and the variation of solar flare from its mean values are shown in the following figures for Feb 15, Oct 2 and Oct 4, 2022.

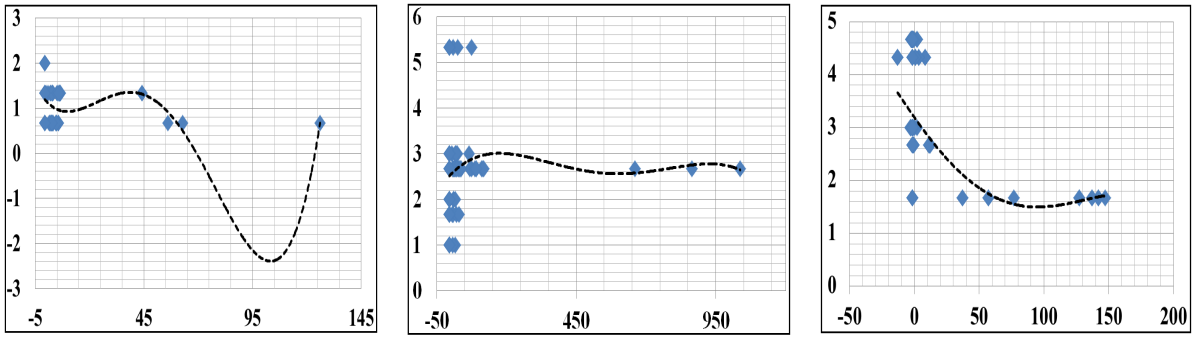

a **b** **c**

Fig.7 Correlation plot of K_p (y-axis) vs. variation of solar flare (x-axis) on (a) Feb 15, 2022, (b) Oct 2, 2022, (c) Oct 4, 2022

The following table (Estimated correlation between K_p and SF) shows the coefficient values at the different orders of the variables present in the polynomial and the correlation coefficient as per expression estimated on the best fitted trend of the parameters.

TABLE VI
ESTIMATED CORRELATION BETWEEN K_p AND SF

Correlated Parameters	Dates	Coefficient values at the different orders of the variables present in the polynomial					Correlation co-efficient
		4^{th}	3^{rd}	2^{nd}	1^{st}	0^{th}	
K_p-SF	Feb 15, 2022	-6×10^{-9}	1×10^{-6}	0.0001	0.0349	3.1943	0.0228
	Oct 2, 2022	-2×10^{-11}	4×10^{-8}	3×10^{-5}	0.0063	2.5428	0.002
	Oct 4, 2022	3×10^{-7}	-7×10^{-5}	0.0037	-0.053	1.1591	0.0115

C. Ionospheric Parameters

The following figure shows the whole day variations of solar flare and the TEC, difference of Ne and N_mF_2 and the solar flare and f_0F_2 and the solar flare for Oct 2, Oct 4 and Feb 15, 2022. The standard deviation and mean of the ionospheric variables are listed in the consequent table.

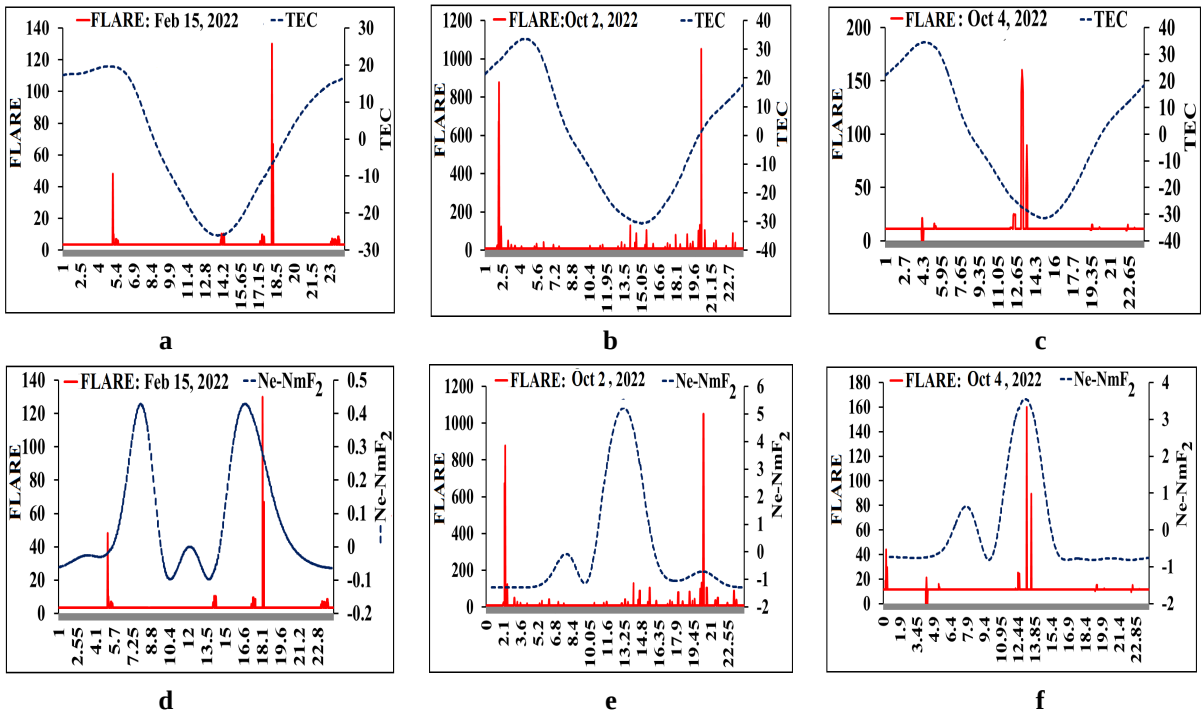

a **b** **c**

d **e** **f**

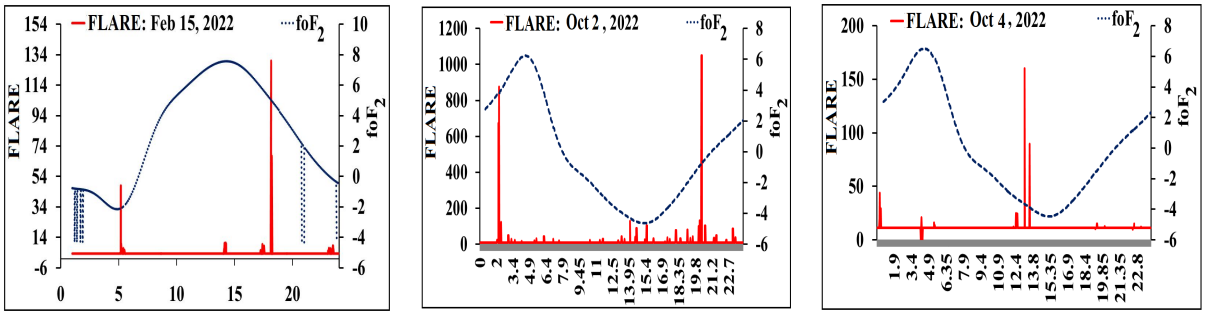

h **i** **j**

Fig. 8 Variations of TEC-Flare magnitudes (a) Feb 15, 2022, (b) Oct 2, 2022, (c) Oct 4, 2022. Variations of Ne-N_mF_2 and Flare magnitudes (d) Feb 15, 2022, (e) Oct 2, 2022, (f) Oct 4, 2022.Variations of f_0F_2 and Flare magnitudes (g) Feb 15, 2022, (h) Oct 2, 2022, (i) Oct 4, 2022 (broken blue lines for the ionospheric parameters and solid red lines for the flares).

TABLE VII
STATISTICAL MEASURES OF THE IONOSPHERIC PARAMETERS

Parameters	Days	TEC	Ne	N_mF_2	f_0F_2
Standard deviation	February 15, 2022	16.20	591393.8	594901.5	3.31
	October 2, 2022	21.49	718918.5	824886.5	3.37
	Oct 4, 2022	22.08	781699.9	836757.8	3.42
Mean	Feb 15, 2022	21.13	780984.8	798495.6	7.31
	Oct 2, 2022	39.62	1380466	1512695	10.52
	Oct 4, 2022	38.84	1418001	1497352	10.44

The following figure shows the variation of diurnal TECs between Feb -15 and Oct- 4, 2022 , Feb- 15 and Oct -2, 2022 and Oct -2 and Oct-4, 2022. The maximum and minimum difference values for the TECs on Feb -15 and Oct- 4, 2022 are 14.6977, -5.4023 respectively and for Feb- 15 and Oct -2, 2022 are 13.91513, -4.58487 and for Oct -2 and Oct-4, 2022 are 0.78257,-0.81743.

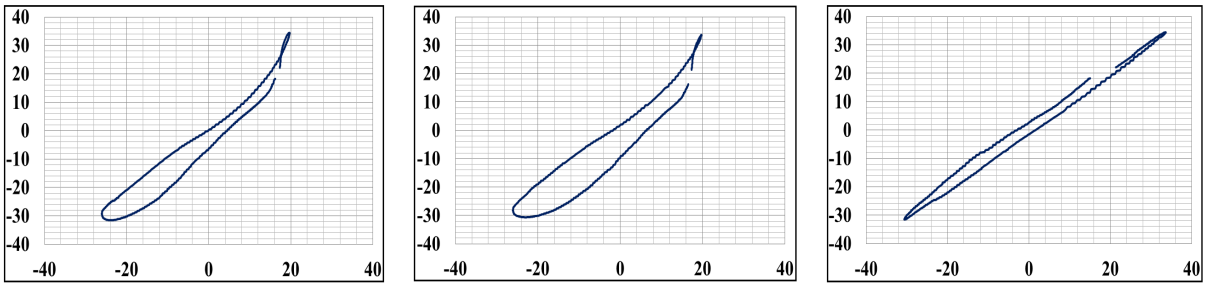

a **b** **c**

Fig.9 Variation of diurnal TECs between of (a) Feb 15, 2022 (x-axis) and October 4, 2022 (y-axis) (b) Feb 15, 2022 (x-axis) and October 2, 2022 (y-axis) (c) October 2, 2022 (x-axis) and October 4, 2022 (y-axis)

The plots represented in Figure 9 significantly show hysteresis between these TEC variation for the pair wise combination of dates. Therefore, it is essentially clear from this observation that temporal flare magnitude variation has a certain leading and lagging effect on the diurnal TEC variations. Depiction of this critical examination of the significant flares to find the hidden transiency between time of variation of flare magnitude and TEC is done in the Figure 10. It shows the differential variation of the TEC**,** N_mF_2 and f_0F_2 *w.r.t.* flare during starting to maximum and maximum to ending for the significant flares happened during October 2 and 4, 2022 and February 15, 2022 and are estimated as the process depicted in data analysis section. In this figure the differential TEC *vs.* flare magnitude variation changes most for the flare C9.2 at its staring time, so the TEC change is higher than the flare magnitude change.

For M1.61 starting and ending time variation is moderate in both the cases TEC change is higher. Approximate same levels of variations are located for the abscissae grazing values like C4.8 and M1. Mild variation with higher TEC change is located for the most effective X1.05 flare for both the time. In case of differential variation of Ne-N_mF_2 to the flare magnitude, the maximum change observed at flare class C4.4. For X1.05 flare this stood as minimum. For other flares moderate and zero grazing variations are observed. In f_0F_2 the more transiency are observed for M1 and C4.8. In case of X1.05, the transiencies are moderate. The maximum to final variation has shown elevated values than the initial to maximum for f_0F_2.

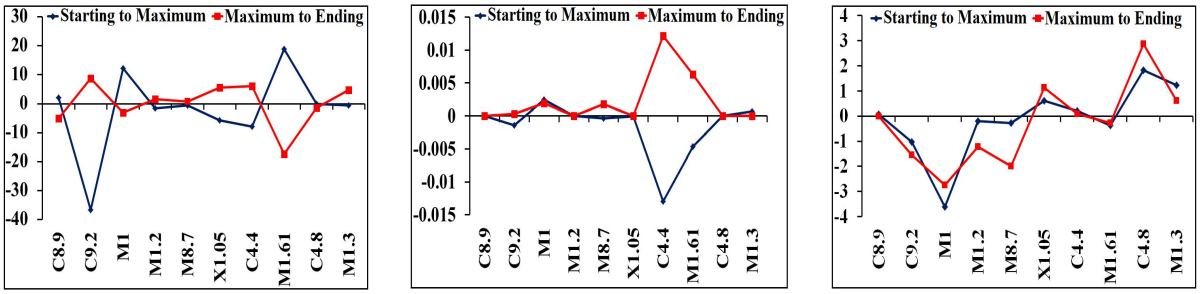

a **b** **c**

Fig.10 Transient variations of differential changes of (a) TEC, (b) NmF_2 and (c) f_0F_2 *w.r.t.* flares magnitudes during starting to maximum and maximum to ending phases for the significant flares happened during October 2, 2022, October 4, 2022 and February 15, 2022.

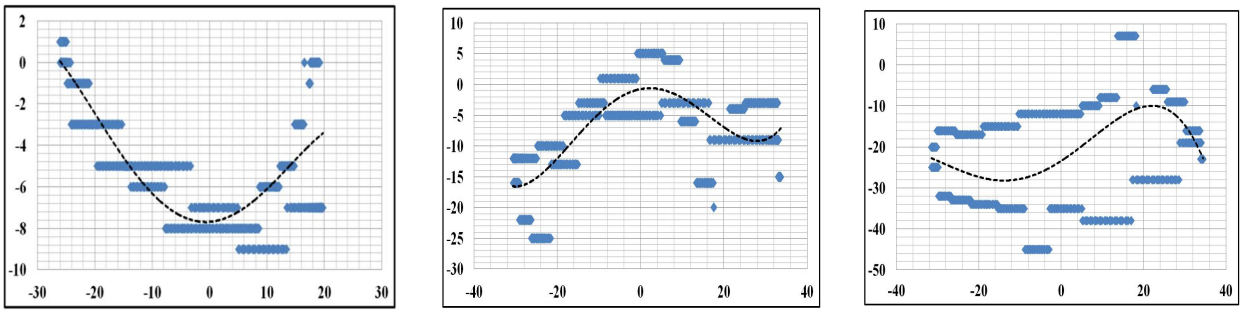

a **b** **c**

Fig.11 Variations of TEC (y-axis) vs. Dst (x-axis) on (a) Feb 15, 2022, (b) Oct 2, 2022, (c) Oct 4, 2022

Figure 11 shows the correlation between Dst index and solar flare on Feb 15, 2022, Oct 2, 2022 and Oct 4, 2022. The dependence nature is shown by the dotted curves. Estimated fitted polynomials and their orders are tabulated in Table 8 and the correlation co-efficient are also shown thereby.

TABLE VIII
ESTIMATED CORRELATION BETWEEN TEC-DST

Correlated Parameters	Dates	Coefficient values at the different orders of the variables present in the polynomial					Correlation co-efficient
		4^{th}	3^{rd}	2^{nd}	1^{st}	0^{th}	
TEC-Dst	Feb 15, 2022	2×10^{-5}	8×10^{-7}	- 0.0286	0.1264	- 0.7524	0.5184
	Oct 2, 2022	-1×10^{-5}	-0.0006	0.017	0.6549	-23.401	0.2281
	Oct 4, 2022	-9×10^{-6}	-0.0001	0.0157	0.0222	-7.6878	0.5533

D. Surface Parameters

The relative diurnal variation of surface parameters for the October 1 to October 5 and February 14 to February 16 with M1.61, M1.3, X1.05 and M8.7 flares happened therein are shown in the Figure 12 with the time duration are in the shaded part. The abscissae are considered as the index value (i.e. Time index =24hrs/30min= 48 points) in time as 06.30 AM to 12 Noon and 12 Noon to 05.30 AM is taken for 30 minutes intervals.

Extracts from these figures are given below.

1) The difference of parameters between the day of flare and the day before after it at the maximum intensity time are estimated to find the exact behaviour of the surface level response at the perturbation generated due to the flare.

2) It is found from these estimation that there is a change in the temperature value of |-0.56| for M1.61 class on October 4, |-3.89| (w.r.t. day before) and |-1.12| (w.r.t. day after) for X1.05 class, |+1.67| for M8.7 class on October 2 flare and no change for M1.3 on Feb 15 respectively.

3) Dew point also shows a depression for X1.05 flare of |-1.11| and |-2.22| respectively. Enhancement in dew-point for the day before and decrement for the day after of the flare day is observed on February 15, 2022. M1.61 and M8.7 shows decrement in this value w.r.t the day after it.

4) Humidity for the X1.0 flare is differed as 11% and -5% for the day before and after it respectively. M1.3 also shows the same kind of variation in this respect. No change in this parameter is observed compared to the previous and next day M1.61.

5) Change in the surface pressure is observed for the X1.05 class as |±1.02| compared to the preceding and the succeeding days. M8.7 class shows slightly larger values of surface pressure depression compared to the next day. M1.61 shows |4.0632| and |-3.0474| and M1.3 shows |-1.0158| and |2.0316| *w.r.t* the day before and after it.

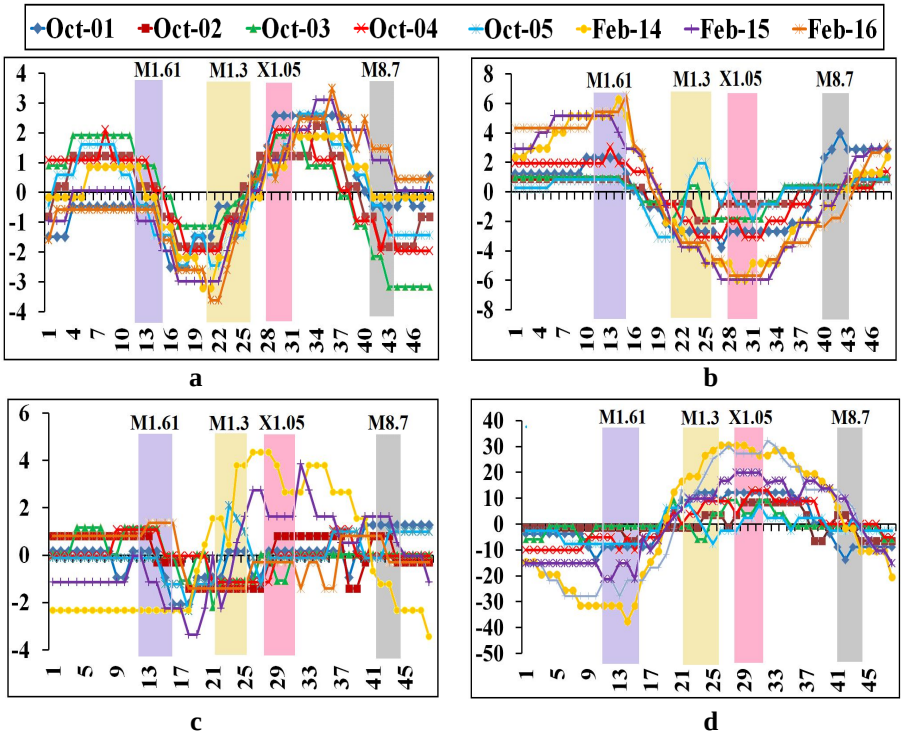

Fig.12 Whole day (Time index along abscissae) relative variations of (a) surface pressure, (b) temperature, (c) dew point and (d) Humidity during Oct 1 to Oct -5 and Feb-14 to Feb-16, 2022. Abscissa represents the time scale index values. The duration of M1.61, M1.3, X1.05 and M8.7 class for flares are demarcated by the coloured shaded region during the period.

E. Findings

1) The contour plot of prediction shows the inactiveness regarding the most geomagnetic disturbances that are located around the October 2, 2022.

2) The geomagnetic storm predictions are significantly satisfied from the geomagnetic activity index analysis as K_p index varies most between October 2-4, 2022 this confirms the unstable geomagnetic field, again the February 15, 2022 shows a slow geomagnetic variation. Dst index variation also supports these somewhat to a reasonable range. Most enhanced standard deviation and mean value appear for October 4, 2022. The effect of solar perturbation due to the flare propagates down form the F_2 to E layer of the ionosphere and that is analyzed by the correlation of the Dst and TEC for the two days. The variation of the ring current in the E layer due to the instantaneous change of the TEC content is shown through the correlations. The correlation co-efficient of these parameters stood highest on the February 15, 2022 but the most promising variation in the trend

line is observed for the October 2, 2022. The 0^{th} and 1^{st} coefficient of the polynomial as derived are stood highest for this. Therefore, a closely related variation between TEC and Dst is observed while the other days have significant contributions of the coefficients for the higher order polynomials.

3) Less correlation between solar flare and K_p index and also co-efficient with lower values are obtained on October 2, 2022. February 15, 2022 shows highest correlations and October 4, 2022 remains in between these two. Linear variation part for October 4, 2022 is most prominent than the other. Most fluctuating trend of K_p-Solar Flare variation is observed for February 15, 2022. The variation in the ionosphere layers are less observed from the K_p and other derived geomagnetic parameters. This can be understood as the K_p is a three hours cumulative index, so the perfect reflection of the short-term changes is not explainable from these observations.

4) The usual TEC variation for daytime shows that the usual enhancement in its value following the decrement in its nighttime value. This pattern will be perturbed by external solar activities like flare and the interacting wind particles then more dissociation in the atoms and large number of electrons and ions for the temporary basis will be generated in ionopsheric layers. Hence, it is expected that this condition will be reflected on the pattern of diurnal variation of TEC with a spike or bulging. It is observed from the results obtained on October 2, 2022 interestingly a bulging in the TEC curve is observed but on February 15, 2022 and on October 4, 2022 no such response is noted.

5) As on October 2 The Earth directed X1.0 class of flare is generated from the vicinity of the sunspot. At the same time duration, this flare a temporary enhancement is TEC value is observed. This can be apprehended as a direct effect of the flare. The other giant of flare M8.7 happened on the same day but has not shown such kind of enhancement in the TEC value.

6) Usually variation of Ne, N_mF_2 and f_0F_2 value forms a trough with a peak at the daytime due to the dissociation of F-layer in F_1 and F_2 part. The density of electron in that layer enhances. The band of critical frequency in the daytime is lower and at the night times its goes higher as the maximum refection height of the ionosphere increases in the daytime. During February 15, October 2 and October 4, 2022 the highest values of them are observed at 14.3 UT, 16 UT and 15.2 UT respectively. Importance of these times is to identify the transiency in growth as more than hourly difference note the time of maximization in their values. The effect maximization of the charge dissociation propagates downward from F_2 layer that placed extremely outside among the ionospheric layer therefore the usual variation of Ne shows delayed response than N_mF_2 after the noontime. This concept is reflected from difference of Ne and N_mF_2. The F_2 layer density crosses the total plasma electron density during this process. In comparison among the three days, the October 4 shows most variation than the others though most of the flare happened on the October 2, 2022.

7) Though Ne-N_mF_2 value shows an instantaneous variation with the appearance of the flare over the usual variation at the occurrence of X1.05 but interestingly a certain enhancement (between 6.8 to 8.4 UT) after the long lapse of time after the passage of M8.7 peak (02.21 UT) is observed. This delay can be interpreted from inertia effect of the ionosphere ions [29] and electrons or may be due to the magnetic reconnection [30,31].

8) Mean of TEC, Ne, N_mF_2 and f_0F_2 on October 2 is largest than the other two days. But the standard variation of these values is recorded for the October 4, 2022 implying the randomness. These may be counted for the X1.0, M8.7 and M1.61 flares happened on those days.

9) The transient variations (Figure 10) of the TEC, N_mF_2 and f_0F_2 at the higher class of flares with more penetrating power to the atmosphere are got zero grazing along the abscissae. Out of all, X1.05 has most penetrating power but during this, the observation refers that the usual variation of the ionopsheric parameters goes into the night side. The critical observation on zero grazing transient variation can be interpreted that the usual time rate change of the parameters has been superposed with the perturbation thereby compelling it slower or rather moreover constant the rates of change. The M8.7 flare lies in the dayside of the ionopsheric variation and slow variation is observed. Other flares are distributed among all the three days with the less magnitude affected least.

10) The few anomalies in N_mF_2 and f_0F_2 is observed for C4.8 and M1.31 flares happened on the Feb 15, 2022. This can be interpreted as the winter seasonal and lower latitude (Tropical region: Indian Ocean region) based anomalies. The month of February fall in the ending part of the winter season so the ionisation in the ionosphere is significantly differs and the molecule to atom ratio is greater and loss in ion lesser than the summer seasons this suggests a low value of plasma frequency of the F_2 layer.

11) Discrepancy in ionospheric parametric variation behaviour during the solar perturbed condition is observed on February 15 as the long filament associated with solar flare and CME are erupted from the solar surface carrying the wind particle but no such activity in the ionsopheric layers is recorded thereof. This unexpected result can be interpreted from the images of SUVI 304 Å,

GOES-17 that appeared approximately 35^0 behind the eastern limb of the Sun and as confirmed by STEREO-A of LASCO C2 and C3 observations [32,33]. Therefore, the eruption side of the Sun is not facing the planet, as it happened on the opposite limb and there is no head-on collision with the ionosphere, so hardly a component of this eruption driven perturbation like enhancement of the radiation, magnetic field and associated wind particles can only manage to reach the Earth surface.

12) The ring current variation *w.r.t* changes in TEC due to the appearance of the large class of flares like X1.05 and M8.7 on October 2, 2022 are interpreted from the Figure 11 between the TECs of February 15, October 2 and October 4. These TECs variation show a curve that shows a hysteresis between the TECs values among the days can be considered. This amount of areal coverage stood highest, least and midway for February 15 and October 2, October 2 and October 4 and February 15 and October 4 respectively.

13) The October 2 covers most of the large kind of flare than other two days so a certain lag between them should be expected. At the full cyclic variation of the TEC throughout the in February 15 pattern shows lagging than October 2 and October 4. On October 2, a momentary slow variation is observed and the approach of curve towards the February 15 is also located.

14) As the effect of flare has to propagate downward direction starting from the ionosphere then stratosphere and then upper and lower troposphere then at last reaches the surface layer. The surface level analysis shows the close insight into the effect of all the four most intensified flares on the surface parameters. The change of surface level parameters mostly affected due to the intervention of the highest intensified X1.05 class as per the expectation. The effect of others also provides significant comparison in this respect. It is observed that surface temperatures and dew-point during maximum flare time of the X1.05 class decreases. Humidity profile and the surface pressure increases from the day before it and decreases for the day after it.

15) As all the above major observations of the ioniospheric parameters show finite responses *w.r.t* this X1.05 class flares. Hence, it can be proposed from these observational insights that to some extent the transitions of the parameters at surface level due to the appearance of that flare and solar-terrestrial coupling are happened.

IV. CONCLUSION

This study demonstrates the profound impact of flares driven associated space weather events on ionosphere and surface weather systems. The comparative analysis of February 15, October 2, and October 4, 2022, reveals distinct solar–terrestrial interaction patterns. Although October 2 experienced minimal geomagnetic disturbance, the Earth-facing X1.0 flare triggered the strongest TEC and F-layer enhancements, with evident ionospheric–surface coupling. The October 4 geomagnetic storm exhibited the highest variability and nonlinear behaviour, poorly captured by K_p alone, and showed the widest Ne–N_mF_2 gap. In contrast, February 15's far-side CME produced limited ionospheric effects despite strong flare activity. Surface variations *viz.* temperature dips and humidity shifts mirrored ionospheric changes. Future work should develop real-time coupling indices and advanced models to improve predictive capabilities.

V. ACKNOWLEDGMENT

We sincerely acknowledge the data sources like NOAA, GSFC-NASA, DSCOVER, IRI-Model, Wyoming University and University of Kyoto for using part their relevant data in the context of this work. Again, we also sincerely acknowledge JIS University to give encouragements and support without that the work would never have been possible.

REFERENCES

[1] R. A. Heelis, A. D. Richmond, and A. Maute, “Magnetic signatures of ionospheric disturbance dynamo for CME and magnetic storm events,” Space Weather, vol. 19, no. 6, e2021SW002825, 2021.

[2] L. A. Hayes, O. S. D. O’Hara, S. A. Murray, and P. T. Gallagher, “Solar flare effects on the Earth's lower ionosphere,” Solar Phys., vol. 296, no. 11, p. 167, 2021. https://doi.org/10.1007/s11207-021-01909-2

[3] S. I. Peykova and A. D. Danilov, “Impacts of ionospheric conductance on magnetosphere–ionosphere coupling during solar geomagnetic storms,” J. Geophys. Res. Space Phys., vol. 127, no. 10, e2022JA030864, 2022. https://doi.org/10.1029/2022JA030864

[4] N. Gopalswamy, S. Yashiro, G. Michalek, G. Stenborg, A. Vourlidas, S. Freeland, and R. Howard, “A catalog of halo coronal mass ejections from SOHO,” Solar Phys., vol. 240, no. 2, pp. 329–351, 2006. https://doi.org/10.1007/s11207-006-0123-y

[5] A. Banerjee, S. Das, and A. B. Bhattacharya, “Sunspot occurrences and the probable effect of interference with HF radio communications in the earth’s ionosphere,” in Proc. 2016 Int. Conf. Comput., Elect. Commun. Eng. (ICCECE), Kolkata, India, Dec. 2016, pp. 1–4. doi: 10.1109/ICCECE.2016.8009582.

[6] NASA, Solar Cycle 25 is heating up, NASA Goddard Space Flight Center, 2022. https://www.nasa.gov/feature/goddard/2022/solar-activity-on-the-rise-solar-cycle-25-heats-up

[7] S. M. White, R. J. Thomas, and R. A. Schwartz, “Updated expressions for solar radio flux density and GOES X-ray flux,” Solar Phys., vol. 227, no. 2, pp. 231–248, 2005. https://doi.org/10.1007/s11207-005-2445-z

[8] A. Banerjee, S. Das, and A. B. Bhattacharya, "Sunspot occurrences and the probable effect of interference with HF radio communications in the Earth's ionosphere," in Proc. 2016 Int. Conf. Comput., Elect. Commun. Eng. (ICCECE), 2016, pp. 1–4. https://doi.org/10.1109/ICCECE.2016.8009582
[9] European Space Agency, Giant solar eruption seen by Solar Orbiter, Feb. 18, 2022. https://www.esa.int/Science_Exploration/Space_Science/Solar_Orbiter/Giant_solar_eruption_seen_by_Solar_Orbiter
[10] D. F. Webb and T. A. Howard, "Coronal mass ejections: Observations," Living Rev. Solar Phys., vol. 9, no. 1, p. 3, 2012. Available: https://doi.org/10.12942/lrsp-2012-3
[11] SpaceWeather.com, "Sunspot AR2941 unleashes M1.3 solar flare causing minor shortwave blackout," Feb. 15, 2022. https://spaceweather.com/archive.php?view=1&day=15&month=02&year=2022
[12] NASA, "Sun releases strong solar flare," NASA Solar Cycle 25, Oct. 2, 2022. https://science.nasa.gov/blogs/solar-cycle-25/2022/10/
[13] NASA Scientific Visualization Studio, Solar flare visualization, SVS, 2022. https://svs.gsfc.nasa.gov/14275/
[14] NOAA Space Weather Prediction Center, "NOAA forecasts G2-class geomagnetic storm due to multiple CME impacts," National Oceanic and Atmospheric Administration, Oct. 4, 2022. https://www.swpc.noaa.gov
[15] SpaceWeather.com, "Multiple CMEs are coming: NOAA forecasters expect G2-class geomagnetic storm today [Archive]," Oct. 4, 2022. https://spaceweather.com/archive.php?day=04&month=10&view=1&year=2022
[16] A. Banerjee and R. Bhattacharya, "On the transient response of the troposphere and ionosphere during annular solar eclipse using radio signal analysis," Geomagn. Aeron., vol. 62, suppl. 1, pp. S142–S158, 2022. https://doi.org/10.1134/S0016793222100048
[17] M. Regi, G. Redaelli, P. Francia, and M. De Lauretis, "ULF geomagnetic activity effects on tropospheric temperature, specific humidity, and cloud cover in Antarctica during 2003–2010," J. Geophys. Res. Atmos., vol. 122, pp. 6488–6501, 2017. https://doi.org/10.1002/2017JD027107
[18] K. A. Nicoll and R. G. Harrison, "Detection of lower tropospheric responses to solar energetic particles at midlatitudes," Phys. Rev. Lett., vol. 112, p. 225001, 2014. https://doi.org/10.1103/PhysRevLett.112.225001
[19] J. J. Curto, "Geomagnetic solar flare effects: A review," J. Space Weather Space Clim., vol. 10, p. 27, 2020. https://doi.org/10.1051/swsc/2020027
[20] A. Sudikin Pramanik, A. Banik, A. Banerjee, and R. Bhattacharya, "Effect of solar flare on ionosphere: a short review," in Proc. Int. Conf. Recent Trends Phys. Allied Sci., vol. 1, no. 1, pp. 24–27, 2023. ISBN: 978-93-89817-84-3.
[21] A. Banerjee, S. Paramanik, A. Banik, A. Bhattacharya and R. Bhattacharya, "On the variation of the solar wind speed with the flare intensity and wind density during X-Class solar flare on June 9, 2023", 5th International Conference on "Physics for sustainable development and Technology", on 7th -8th September, 2023, Department of Physics, Chittagong University of Engineering & Technology (CUET), Bangladesh, published in Book of Abstract, id-128, p-95.
[22] S. Pramanik, A.Banik, A. Banerjee and R. Bhattacharya, "A study on relationship between Solar perturbations and Tropical cyclonic events", Abstract Proceedings National seminar on climatic change: Water security Across Generation, Department of physics and Department of Geography, Dukhulal Nabin Chndra College in collaboration with Indian Meteorological Society, Alipur, Kolkata, March 22, 2023. ISBN-978-93-89871-84-3.
[23] G. E. Brueckner, R. A. Howard, M. J. Koomen, C. M. Korendyke, D. J. Michels, J. D. Moses, D. G. Socker, K. P. Dere, P. L. Lamy, A. Llebaria, M. V. Bout, R. Schwenn, G. M. Simnett, D. K. Bedford, and C. J. Eyles, "The Large Angle Spectroscopic Coronagraph (LASCO)," Solar Phys., vol. 162, no. 1–2, pp. 357–402, 1995. https://doi.org/10.1007/BF00733434
[24] J. R. Lemen, A. M. Title, D. J. Akin, P. F. Boerner, C. Chou, J. F. Drake, D. W. Duncan, C. G. Edwards, F. M. Friedlaender, G. F. Heyman, N. E. Hurlburt, N. L. Katz, G. D. Kushner, M. Levay, R. W. Lindgren, D. P. Mathur, S. McFeaters, S. Mitchell, R. A. Rehse, C. J. Schrijver, L. A. Springer, R. A. Stern, T. D. Tarbell, J.-P. Wuelser, and L. Yanari, "The Atmospheric Imaging Assembly (AIA) on the Solar Dynamics Observatory (SDO)," Solar Phys., vol. 275, no. 1–2, pp. 17–40, 2012. https://doi.org/10.1007/s11207-011-9776-8
[25] NASA, "Cannibal CME triggers rare pink auroras," NASA Science Blog, Nov. 7, 2022. https://blogs.nasa.gov/solarcycle25/2022/11/07/cannibal-cme-triggers-rare-pink-auroras/
[26] Y. Nishimura, L. R. Lyons, V. Angelopoulos, and Y. Miyoshi, "Substorm triggering by new plasma intrusion: THEMIS all-sky imager observations," J. Geophys. Res. Space Phys., vol. 115, A07222, 2010. https://doi.org/10.1029/2009JA015166
[27] NASA, "Pulsating auroras driven by magnetospheric 'chorus' waves," NASA Science News, May 23, 2018. https://www.nasa.gov/feature/goddard/2018/pulsating-aurora-mystery-solved
[28] SpaceWeather.com, "Pink, pulsating auroras in Abisko National Park, Sweden [Photograph by Miquel Such]," in Daily Sun: 04 Oct 22, Oct. 4, 2022. https://spaceweather.com/archive.php?day=04&month=10&view=1&year=2022
[29] M. C. Kelley, The Earth's Ionosphere: Plasma Physics and Electrodynamics, 2nd ed. San Diego, CA, USA: Academic Press, 2009.
[30] M. Yamada, R. Kulsrud, and H. Ji, "Magnetic reconnection," Rev. Mod. Phys., vol. 82, no. 1, pp. 603–664, 2010. https://doi.org/10.1103/RevModPhys.82.603
[31] A. Banerjee and R. Bhattacharya, "Solar Wind Speed Variations as Precursor Through X Class Flare Intensity and Wind Density: A Radio Data Analysis," Indian J. Sci. Technol., vol. 18, no. 6, pp. 403–414, 2025. https://doi.org/10.17485/IJST/v18i6.1506
[32] M. Mierla, A. N. Zhukov, D. Berghmans, S. Parenti, F. Auchère, P. Heinzel, D. B. Seaton, E. Palmerio, S. Ejčič, J. Janssens, E. Kraaikamp, B. Nicula, D. M. Long, L. A. Hayes, I. C. Jebaraj, D.-C. Talpeanu, E. D'Huys, L. Dolla, S. Gissot, J. Magdalenić, L. Rodriguez, S. Shestov, K. Stegen, C. Verbeeck, S. Sasso, M. Romoli, and V. Andretta, "Prominence eruption observed in He II 304 Å up to >6 R⊙ by EUI/FSI aboard Solar Orbiter," Astron. Astrophys., vol. 662, p. L5, 2022. https://doi.org/10.1051/0004-6361/202244020
[33] A. Banerjee, S. Roy, P. Barnal, and R. Bhattacharya, "Variability of the solar, geomagnetic and surface parameters during prominent solar flare on February 15, 2022," in Proc. One Week Workshop on Research Methodology and Practices, JIS University, 2022, p. 19. ISBN: 978-81-957179-6-5.

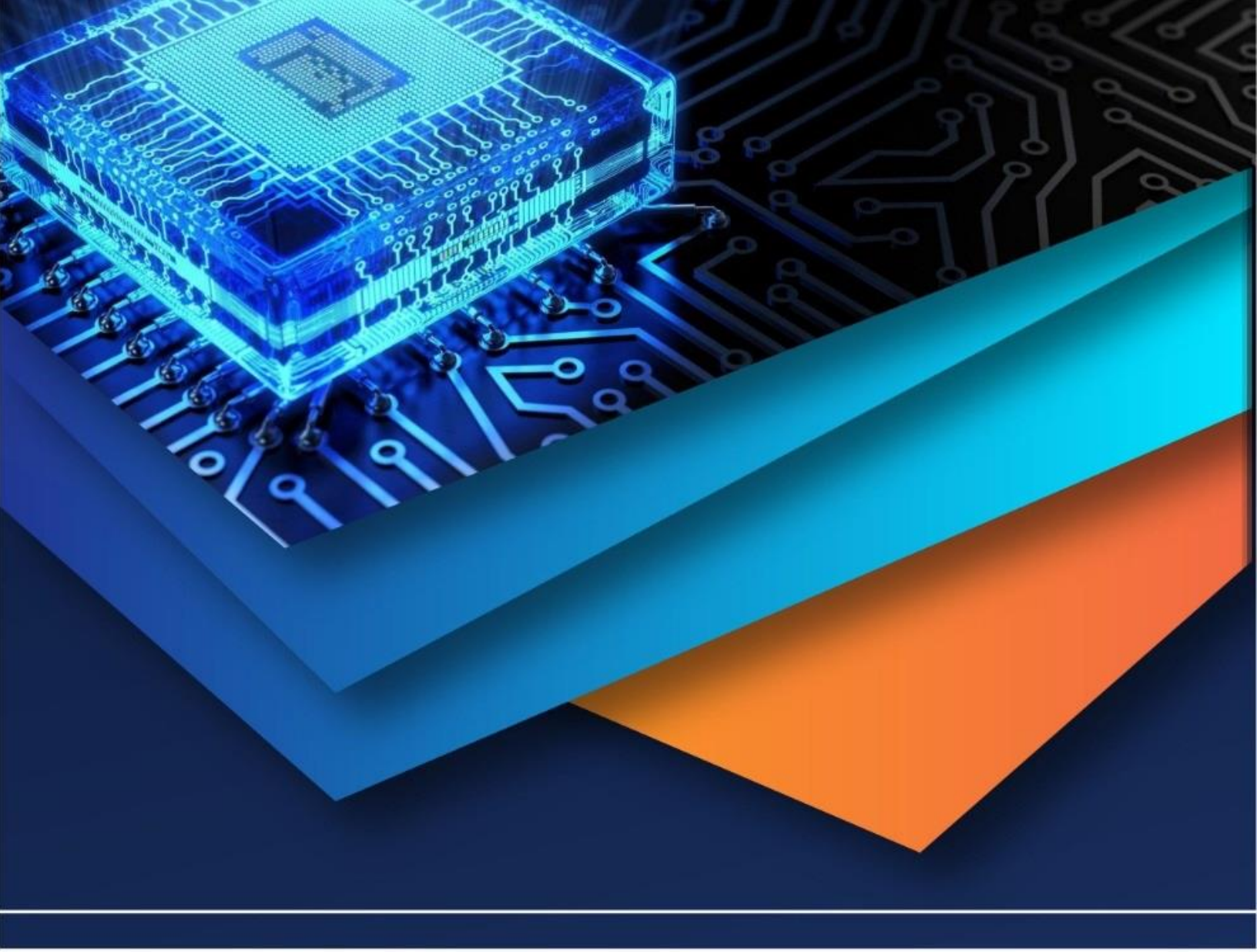

10.22214/IJRASET

45.98

IMPACT FACTOR: 7.129

IMPACT FACTOR: 7.429

INTERNATIONAL JOURNAL FOR RESEARCH

IN APPLIED SCIENCE & ENGINEERING TECHNOLOGY